Hindawi
International Journal of Aerospace Engineering
Volume 2020, Article ID 2676210, 14 pages
https://doi.org/10.1155/2020/2676210

Research Article

A Novel Inertial-Aided Star Pattern Matching Method for Distributed Multiple FoVs

Rong Wang, Yuxuan Cao, Jianye Liu, and Zhi Xiong

Navigation Research Center, College of Automation Engineering, Nanjing University of Aeronautics and Astronautics, Nanjing 211106, China

Correspondence should be addressed to Rong Wang; rongwang@nuaa.edu.cn and Zhi Xiong; xiongzhi@nuaa.edu.cn

Received 24 November 2019; Revised 15 July 2020; Accepted 18 July 2020; Published 6 August 2020

Academic Editor: Angelo Cervone

An aerospace vehicle in high-speed flight involves distributed multiple fields of view (FoVs) of a star sensor, and the maneuvering of the vehicle requires inertial-aided star pattern matching. Accordingly, an inertial-aided star pattern matching method for distributed multiple FoVs is proposed. First, the observation and fusion principles of distributed multiple FoVs are illustrated. Then, an inertial-aided star pattern matching scheme is designed based on the space-time distribution of the line-of sight (LoS) vector and inertial measurement information. Next, an LoS vector estimation method assisted by inertial information and the dynamic establishment of a distributed local catalog are proposed. Finally, in a simulation, the dynamic establishment of the part catalog improves the efficiency of star pattern matching by reducing the catalog scale, and the usability of inertial-aided star pattern matching is analyzed for different gyro and accelerometer precisions.

1. Introduction

An aerospace vehicle is a kind of advanced reusable vehicle for the future [1]. The multitask mode and maneuvering of an aerospace vehicle have considerable requirements in terms of autonomous navigation. In aviation, the celestial navigation system (CNS) plays an important role and has the advantages of autonomy, highly accurate angle measurements, and nonaccumulating error over time.

An analogy can be made between the CNS in the cruise stage of an aerospace vehicle and the small-aperture star sensor that is applied in autonomous identification in a long-range and long-endurance vehicle (LRLEV), where a small-volume sensor and availability during the day and night are ensured [2]. The second-generation CCD star sensor truly realizes full-day autonomous identification without prior information and has the function of " input starlight and output attitude" [3, 4]. At present, the industrialized series production of star sensors has been formed, and the main products are concentrated in the second-generation CCD star sensors and APS CMOS star sensors [5]. Researchers have studied the optimization and improvement of the triangle matching algorithm. The original Danish University of Technology Liebe proposed a method of storing star distance instead of storing triangle features [6]. A star identification algorithm with star ID shortlisting is researched, in which the star IDs are shortlisted based on worst-case patch mismatch, and stars are identified in the image by an initial match confirmed with a running sequential angular match technique [7]. The star pattern identification algorithm using the vector pattern matching technique on the celestial sphere is also researched, which is formed by the correlation between the original and the reference star patterns on the celestial sphere [8]. The star identification algorithm is researched for the attitude determination of a star sensor in the lost-in-space case, which uses label values to represent each group of stars [9]. A set of lost-in-space star identification algorithms that work effectively for small satellites was proposed [10]. However, a small-FoV star sensor is limited by a small number of visible stars, identifies centrally distributed stars, and requires frame control. In addition, the LRLEV aerospace vehicle has a higher flight speed. In this way, the installation location of the star sensor is constrained further, and multiple FoVs exist in a noncontinuous

distribution, which results in visible stars with a poor geometric structure [11]. Therefore, the above issues mean that a single small-aperture star sensor cannot provide continuous and robust navigation information for an aerospace vehicle in flight.

Multi-FoV fusion technology can extend the visible area and focus the stars in different FoVs, increasing the number of visible stars and improving the geometric structure of the identified stars [12]. In recent research on a multi-FoV fusion all-sky identification algorithm, Texas A&M University proposed the pyramid algorithm in [13], which identifies a feature based on the star vector inner product of 4 stars, and the SP search algorithm in [14], which searches a spherical polygon in a wide-FoV star sensor. These two algorithms were employed to achieve successful star identification with multi-FoV fusion in an orbit vehicle in [15]. In addition, the applications of mass production multi-FoV star sensors, such as HYDRA [16] and DECOM [17], provided a reference for aerospace vehicle aviation.

For an aerospace vehicle with a large turning angle and angular rate, the positions and attitudes from the single CNS have a large error so that only a star tracking algorithm, such as an interframe estimation algorithm, that does not depend on the external navigation information will be more likely to lose lock [18]. Later, the all-sky identification algorithm rapidly recovers the output because of the calculation cost. However, both the CNS and an inertial navigation system (INS) are autonomous navigation systems, and a navigation system integrating these systems can exhibit complementary advantages suitable for the autonomous navigation of an aerospace vehicle. In recent research on a star identification algorithm assisted by an INS, a recursive star identification algorithm used a gyroscope to aid the attitude estimation in [19]; an INS-assisted algorithm estimated the LoS vector with the positions and attitudes from the INS in [20]; and a fast star identification algorithm provided preliminarily analysis of the influence of inertial measurement information. On the basis of these three results, an INS-assisted star identification algorithm can address the problem of a large maneuver in flight through theoretical analysis and an efficient verification of the inertial measurement error in star identification.

The perspective inertial-aided approaches for star tracker mainly focused on single FoV. The star sensor with multiple FoVs shows advantage than a single FoV, while stars within the same FoV and across different FoVs are both adopted, so the appropriate inertial-aided approaches need to be investigated. With multiple small distributed FoVs on the aerospace vehicle and the method of star identification assisted by inertial measurement information mentioned above, an inertial-aided star pattern matching method for distributed multiple FoVs is proposed. First, star image fusion under distributed multiple FoVs and an invisible area is analyzed, marking the beginning of the imaging principle of multiple FoVs. Then, an inertial-aided star pattern matching process is proposed based on the spatiotemporal relationship between the LoS vector and the inertial measurement information. Next, multi-LoS vector estimation and the dynamic establishment of a star part catalog are presented, and the inertial-aided star pattern matching method is researched. Finally, the influence of inertial measurement units with different accuracies on aided matching is analyzed, and the results show that aided matching has a higher efficiency due to the scale reduction of the part catalog. The main contribution of this paper lies in two aspects: Firstly, an inertial-aided dynamic predicting method for multiple FoVs' observed scopes is proposed, in which the biases caused by the errors of inertial navigation system are taken in consideration, respectively. Secondly, a star pattern matching based on predicted local star catalog is proposed, whose magnitude is significantly reduced and the real-time performance is improved than the conventional star pattern matching method based on all-sky star catalog.

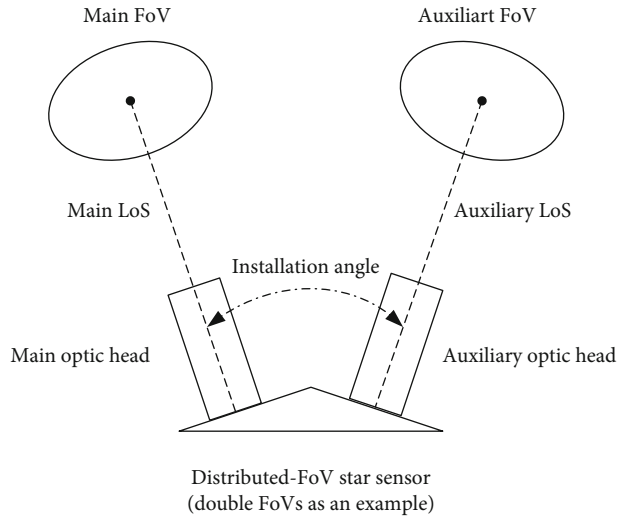

Figure 1: Diagram of a distributed multi-FoV star sensor system.

2. Modeling of Novel Star Sensor with Distributed Multiple FoVs

2.1. Framework of Novel Star Sensor with Distributed Multiple FoVs. The flight of an aerospace vehicle includes the aerospace vehicle taking off, landing, and cruising. In the cruise stage, an analogy can be made between an LRLEV with a small-aperture star sensor. The star sensor for an aerospace vehicle should involve distributed multiple FoVs, such that the FoVs do not overlap. A diagram is shown in Figure 1.

With the core of a multi-FoV star sensor, a CNS can address the problem of aviation usability, but it faces some new challenges. In the existing studies of star identification algorithms with multiple FoVs, the methods of star image fusion and star catalog generation involve continuous multiple FoVs with a small installation angle, and the studies do not present further application analysis of distributed multiple FoVs. In particular, the catalog scale of the multiple FoVs would be larger than that of a single FoV because of the star selection with large angular distance with respect to the setting angles and FoVs. The catalog

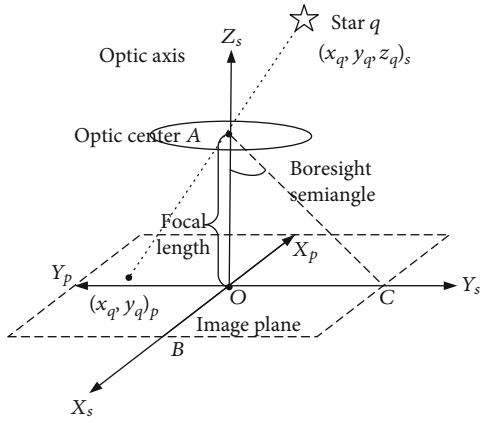

FIGURE 2: Imaging of a single-FoV star sensor.

scale cannot satisfy the efficiency required by aerospace vehicles.

Therefore, the design of a CNS should include a full consideration of the influence of distributed multiple FoVs on the star image and the influence of inertial assistant information on star pattern matching. The identification scheme, a star image observation model, and an image fusion method with distributed multiple FoVs, LoS vector estimation, and the dynamic establishment of a part catalog are researched below.

2.2. Model of a Single FoV in Star Sensor. A star sensor is a sensor that observes and identifies navigation stars. The optical structure of a single-FoV star sensor can be simplified into two parts: a lens and an image plane, which are shown in Figure 2.

Define the coordinate system about the star sensor as follows:

(1) The optic head coordinate system (abbreviated as the s system) takes the image plane center O as the coordinate origin, the LoS vector as the Z axis direction, and the directions of the two vertical sides of the image plane as other axis directions. In terms of a single-FoV star sensor, there is only one s system, which can be called the star sensor coordinate system

(2) The image plane coordinate system (p system) takes the image plane center O as the coordinate origin and the directions of the two vertical sides of the image plane as other axis directions

In Figure 2, the distance $|OA|$ is denoted by the focal length from the optic center A to the image plane, and the line $\overrightarrow{OZ}$ is the optic axis. The size of the star sensor FoV can be regarded as the range observed in the celestial sphere, which is generally described by an angle.

According to the definitions of the coordinate systems above, a star imaging model for a single optical head can be built. Here, a single star is used to describe the imaging process. It is assumed that the coordinate of a star q in the s system is $(x_q, y_q, z_q)_s$. Through a transmission projection, the coordinate of the star q in the p system is $(x_q, y_q)_p$ given in equation (1):

$$\begin{cases} (x_q)_p = -F\dfrac{(x_q)_s}{(z_q)_s}, \\ (y_q)_p = -F\dfrac{(y_q)_s}{(z_q)_s}, \end{cases} \tag{1}$$

where F is the focal length of the optic head.

2.3. New Model for Star Image Fusion between Distributed Multiple FoVs. In the cruise stage of an aerospace vehicle with high speed, the setting of the angle of the multi-FoV star sensor would be constrained due to the strong aerooptical effect. In most cases, multiple optic heads would be installed with large angles to overcome the poor geometric configuration of stars. A double-FoV star sensor is chosen as an example in this section, and the imaging diagram is shown in Figure 3, where the area observed by the main optic head is the area Am, and the area Aa is observed by the auxiliary optic head. The invisible area is not observed by the double optical head. That is, the two FoVs do not overlap.

For multiple FoVs, one optic head corresponds to the s system. The main optic head coordinate system (left) is denoted as the s_1 system, and the auxiliary optic head coordinate system (right) is denoted as the s_2 system. There are two p systems: the main image plane coordinate system (p_1 system) and the auxiliary image plane coordinate system (p_2 system). Analogously to the imaging principle in Section 3.1, two stars are used to describe the imaging process for the distributed double-FoV system. It is assumed that there are two stars q_1 and q_2 observed by the main and auxiliary optic heads, respectively. Their coordinates in the s_1 and s_2 systems are $(x_{q_1}, y_{q_1}, z_{q_1})_{s_1}$ and $(x_{q_2}, y_{q_2}, z_{q_2})_{s2}$, respectively. Through a transmission projection, their coordinates in the imaging planes are

$$\begin{cases} \left(x_{q_1}\right)_{p1} = -F_1\dfrac{\left(x_{q_1}\right)_{s_1}}{\left(z_{q_1}\right)_{s_1}}, \\ \left(y_{q_1}\right)_{p1} = -F_1\dfrac{\left(y_{q_1}\right)_{s_1}}{\left(z_{q_1}\right)_{s_1}}, \\ \left(x_{q_2}\right)_{p_2} = -F_2\dfrac{\left(x_{q_2}\right)_{s_2}}{\left(z_{q_2}\right)_{s_2}}, \\ \left(y_{q_2}\right)_{p_2} = -F_2\dfrac{\left(y_{q_2}\right)_{s_2}}{\left(z_{q_2}\right)_{s_2}}, \end{cases} \tag{2}$$

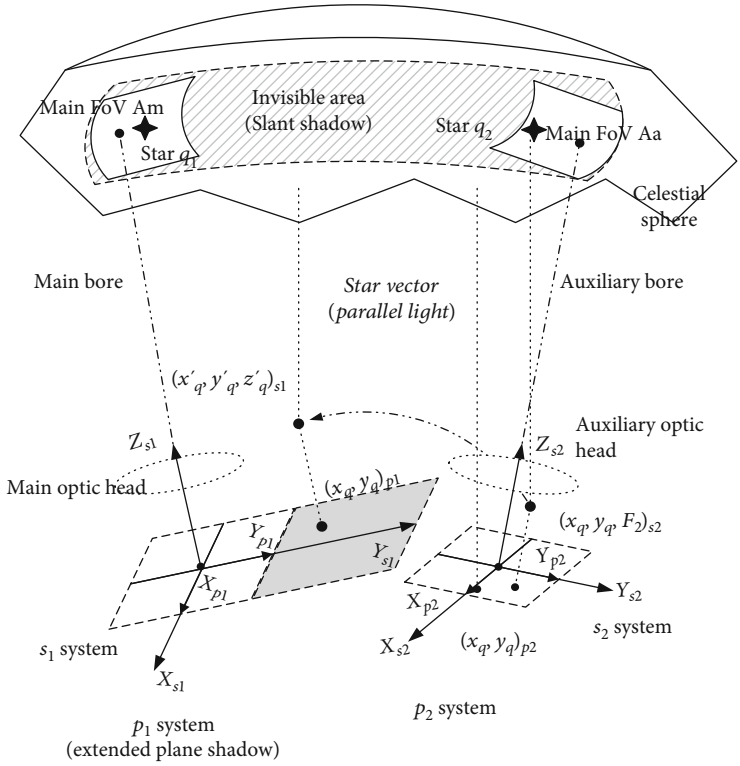

Figure 3: Star imaging diagram for distributed FoVs.

where F_1 and F_2 are the focal lengths of the main and auxiliary optic heads, respectively.

The coordinates and magnitudes of invisible stars can be obtained by star image preprocessing. For a small multi-FoV star sensor, star image fusion is the process of transferring the stars in the auxiliary FoV to the main or extended FoV. From Figure 4, the two FoVs do not overlap, and there could be a large invisible area. Thus, they cannot be mosaicked. To address the problem for distributed multiple FoVs with a large setting angle, a new star image fusion method is proposed. First, the coordinates of the stars in the s system are rebuilt according to the focal lengths. Second, the stars in the s_2 system are transformed into the s_1 system, and third, they are projected into the extended plane of the main image plane.

The star image fusion process is shown in Figure 4. Because the stars are far from the Earth, their light can be regarded as parallel light. The fused star image contains two parts: one part involves the star points that are observed by the main optic head and projected, and the other part involves the star points that are observed by the auxiliary optic head and transformed. The double-FoV star sensor is used to illustrate the fusion process. In Section 3.2, the coordinates of the star point in the auxiliary image plane are obtained and regarded as $(x_{q_2}, y_{q_2})_{p_2}$ by equation (2), which can be rebuilt into the s_2 system by the focal length and can be regarded as $(x_{q_2}, y_{q_2}, F_2)_{s2}$.

When a star sensor with multiple FoVs is strapped to an aerospace vehicle, the installation matrices describe the relationship between the optical heads and the vehicle body. If the matrices of the main and auxiliary optic heads are regarded as $C^b_{s_1}$ and $C^b_{s_2}$, the matrix $C^{s_1}_{s_2}$, which describes the transformation of the two s systems, is given by equation (3):

$$C^{s_1}_{s_2} = \left(C^b_{s_1}\right)^T C^b_{s_2}. \tag{3}$$

The coordinates of the star point $q_2(x'_{q_2}, y'_{q_2}, z'_{q_2})_{s1}$ in the s_1 system after the transformation can be obtained by equation (4):

$$\begin{bmatrix} x'_{q_2} \\ y'_{q_2} \\ z'_{q_2} \end{bmatrix}_{s1} = C^{s_1}_{s_2} \begin{bmatrix} x_{q_2} \\ y_{q_2} \\ F_2 \end{bmatrix}_{s2}. \tag{4}$$

Through the projection, the star point q_2 in the p_1 system is shown in equation (5):

$$\begin{cases} \left(x_{q_2}\right)_{p1} = -F_1 \dfrac{x'_{q_2}}{z'_{q_2}}, \\ \left(y_{q_2}\right)_{p1} = -F_1 \dfrac{y'_{q_2}}{z'_{q_2}}. \end{cases} \tag{5}$$

All the stars in the auxiliary FoV can be transformed by the fusion method above, and the method is not limited to image fusion with double FoVs.

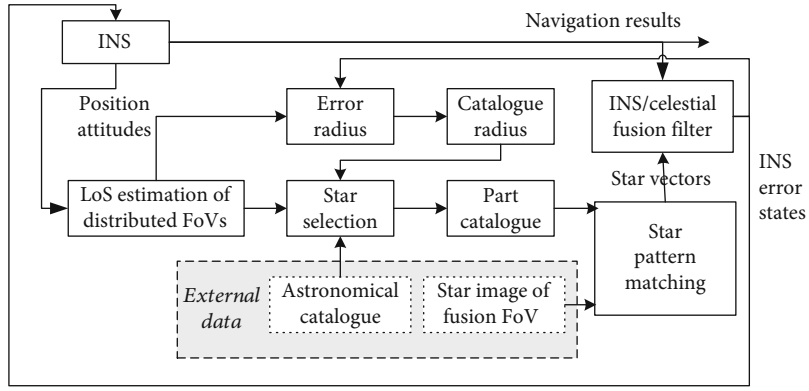

Figure 4: Inertial-aided star pattern matching scheme for distributed FoVs.

3. Novel Inertial-Aided Star Pattern Matching Method for Distributed Multiple FoVs

3.1. Scheme Design. A star catalog contains the possible stars that can be observed by a star sensor. The catalog is preset before star pattern matching and is not changed in the all-sky identification. Assistance identification by external information is a method that utilizes external information with errors to estimate the LoS of the star sensor in real time and constantly maintains a part catalog with a small scale before star pattern matching. The whole scheme is shown in Figure 4.

Figure 4 shows the whole process of the method. It is shown that inertial information helps to estimate the LoS vectors of distributed multiple FoVs, and the errors are calculated as the error radius before the catalogue radius, which helps to select stars and constantly maintain the part catalog. The bias of the calculated LoS vector, caused by the errors in the inertial measurements, could be estimated by the error states of the inertial navigation system. Since the proposed star pattern matching approach is designed for the scenario that stars tracking was just failed and the star sensor could not assist the inertial navigation system during a short episode, the error states of the inertial navigation system could be predicted by time update of its error model in the inertial/celestial fusion filter approximately. Once the stars are retracked after star pattern matching, the measurement update of the fusion filter could be carried out to correct the inertial navigation system again. Thus, the bias information during the star pattern matching episode could be obtained.

3.2. Prediction of the Optical Axis Direction Based on Inertial Measurements. Star identification assisted by an INS for a single-FoV star sensor was studied in [21]. The LoS vector estimation method can be applied to a multi-FoV star sensor. It is assumed that the star sensor has N_B distributed FoVs sorted from 1 to N_B. Obviously, each installation matrix $C_{s_n}^b$ is certain. In theory, the nth LoS vector r_n^i $(1 \le n \le N_B)$ is estimated by equation (6):

$$r_n^i = C_e^i C_n^e C_b^n C_s^b r^{s_n}. \tag{6}$$

Actually, the real LoS vector will be affected by the errors in the inertial information as shown in equation (7):

$$\tilde{r}_n^i = C_e^i \tilde{C}_n^e \tilde{C}_b^n C_s^b r^{s_n}. \tag{7}$$

3.3. Prediction of Multiple FoVs' Observed Scopes. The matrices $\tilde{C}_n^e$ and $\tilde{C}_b^n$ contain the errors. When the errors are small, they are shown in equations (8) and (9) [22]:

$$\tilde{C}_b^n = C_b^n (I - [\phi \times]), \tag{8}$$

$$\tilde{C}_n^e = (I + [\Delta P \times]) C_n^e, \tag{9}$$

where ϕ is the platform error angle vector defined in the navigation system (ENU), $\Delta P = [-\Delta L \, \Delta\lambda \cos L \, \Delta\lambda \sin L]^T$ is the error vector from the position, and δL is the latitude error and $\delta\lambda$ is the longitude error. The inertial errors are derived from the INS error equations.

Inserting equations (8) and (9) into equation (7) and comparing the simplified result with equation (6), the LoS estimation bias ψ_n of the nth FoV can be obtained as follows:

$$\psi_n = \tilde{C}_b^n (\phi - \Delta P). \tag{10}$$

According to equation (9), ψ_n is a rotation Euler vector, giving the rotation between the real LoS vector (without errors) and the estimated LoS vector (with errors) of the nth FoV. It can also be defined as a unique bias angle η_n for ψ_n. If the estimated LoS vector $\tilde{r}_n^i$ is obtained, there is another vector r_0^i that is on the cone generatrix whose cone line is the estimated LoS $\tilde{r}_n^i$ and cone angle is η_n. Thus, the vector r_0^i for the estimated LoS vector $\tilde{r}_n^i$ by equation (7) is given by equation (11):

$$r_0^i = (I + (\psi_n \times)) \tilde{r}_n^i. \tag{11}$$

Then, the LoS bias angle η_n can be calculated by equation (12).

$$\eta_n = d_{r_0^i \tilde{r}_n^i} = \arccos\left(\frac{r_0^i \cdot \tilde{r}_n^i}{|r_0^i| \cdot |\tilde{r}_n^i|}\right). \tag{12}$$

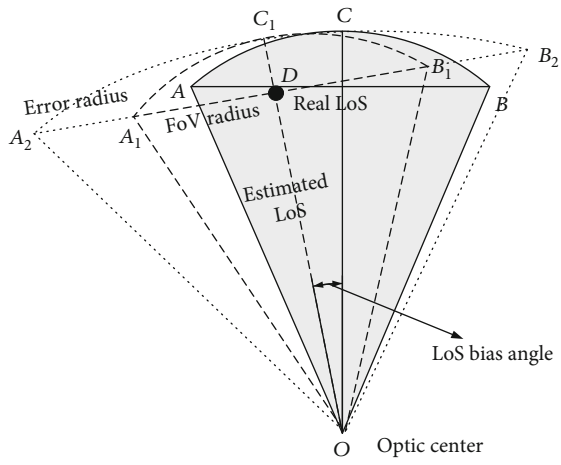

Figure 5: Inertial error analysis for the FoV.

The relationship between the estimated and real LoS is shown in Figure 5. The point O is the optic center, and $\overline{OC}$ is the real LoS vector. The arc $\overset{\frown}{ACB}$ is the real visible range of the star sensor. The errors from the inertial information are small, so the LoS bias angle is also small. Therefore, $\overline{OC_1}$ is the estimated LoS, and$\angle C_1OC$ is the LoS bias angle. The visible range becomes the arc $A_1\overset{\frown}{C_1}B_1$. The inertial errors concern the error radius $\overline{A_2A_1}$ so that the catalog radius $\overline{A_2D}$ contains the FoV radius $\overline{A_1D}$ and the error radius. In this way, the range of the catalog is the arc $A_2\overset{\frown}{C_1}B_2$.

In fact, the celestial sphere area observed by the star sensor is very small and can be regarded as a plane. If the LoS bias angle is small, the celestial sphere area with error is still approximately a plane. Therefore, the LoS bias angle can only affect the range of the catalog.

If the LoS bias angle is written as η_n, then the error radius can be given by equation (13):

$$\Delta R_n = \sin \eta_n. \tag{13}$$

In other words, from equations (3)–(13), each real LoS vector $\tilde{r}_n^i$ and error radius ΔR_n can be calculated.

With the assistance of LoS vector estimation and error radius certainty, the stars in the part catalog are approximately equal to those in the star image. For Section 4.2, the error radius for the nth FoV is written as ΔR_n, and the catalog radius $\tilde{R}_n$ is given by equation (14):

$$\tilde{R}_n = R_n + \Delta R_n. \tag{14}$$

The part catalog is established with the estimated LoS vector and the catalog radius. The method for generating the part catalog has two parts: one part involves star selection, and the other part involves the pattern structure.

One star is used to illustrate the star selection method. If the estimated LoS vector is written as $\tilde{r}_n^i$ and the catalog radius is $\tilde{R}_n$ for the nth FoV, the condition for star q in the nth FoV is shown in equation (15):

$$d_{\tilde{r}_n^i q} \le \tilde{R}, \tag{15}$$

where $d_{\tilde{r}_n^i q}$ indicates the argument between the star q and the estimated LoS vector $\tilde{r}_n^i$. Equation (15) is used to select stars in an all-sky catalog and choose the stars in each FoV.

3.4. Star Pattern Matching Based on Predicted Local Star Catalog. The pattern of the catalog depends on the star identification algorithm. A triangle matching algorithm is chosen, and the pattern is based on the angular distance between the stars. The catalog structure of packet storage for a single FoV in [18] is employed, and the section below analyzes the extended application of distributed FoVs.

However, unlike traditional star sensor with single-FoV, the angular distances between the stars show different characters for star sensor with distributed multiple FoVs.

In Figure 6, there is not only angular distance between the stars within the same FoV but also angular distance between the stars across different FoVs. Thus, two situations are taken in consideration according to the angular distances between stars during the star pattern matching:

(1) Angular distance within a single FoV: the star sets are obtained by the star selection. The nth set is written as $\{\text{star}\}_n$ and the argument set in each $\{\text{star}\}_n$ is $\{d_{pq}\}_n$. For a star sensor with multiple distributed small FoVs, the FoV size is smaller than the installation angle for each optical head, and generally, each FoV has the same size. Therefore, the angular distance of each FoV together form the whole argument set $\{\{d_{pq}\}_n\}$ $(1 \le n \le N_B)$

(2) Angular distance across a pair of FoVs: each star set $\{\text{star}\}_n$ is selected, and then the set with a number larger than n is selected. The angular distance across each two FoVs is calculated. The calculation process is as follows: If a star set $\{\text{star}\}_n$ with number n is chosen, then the following sets with a number from $n+1$ to N_B are chosen to calculate the angular distance. If there is a following set $\{\text{star}\}_m (n+1 \le m \le N_B)$, then the argument is written as $d_{(p)_n(q)_m}$. Accordingly, the argument set is written as $\{d_{(p)_n(q)_m}\}_{nm}$. According to the calculation, the argument sets $\{d_{(p)_n(q)_m}\}_{nm}$ for each two FoVs and the whole set $\{\{d_{(p)_n(q)_m}\}_{nm}\}$ can be obtained

The two argument sets have different values. One needs to choose the appropriate argument value as the grouping interval as in reference [18]. The two sets are divided into intervals, and the argument patterns are all based on packet storage. These patterns make up the part catalog. The whole catalog is shown in Figure 7.

With the combination of the inertial-aided star identification scheme (Figure 1) and the part catalog, the inertial-

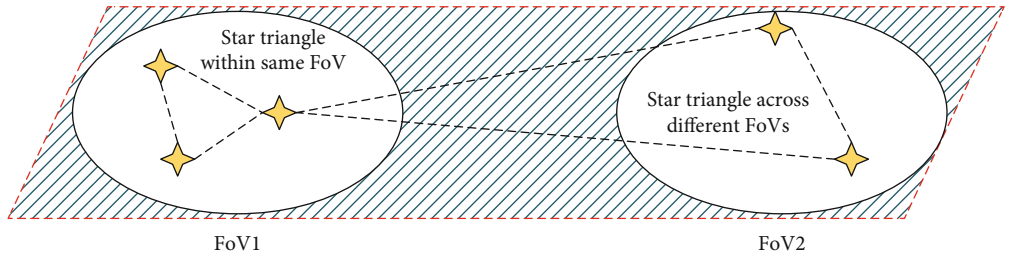

Figure 6: Two situations of the angular distances for distributed multiple FoVs.

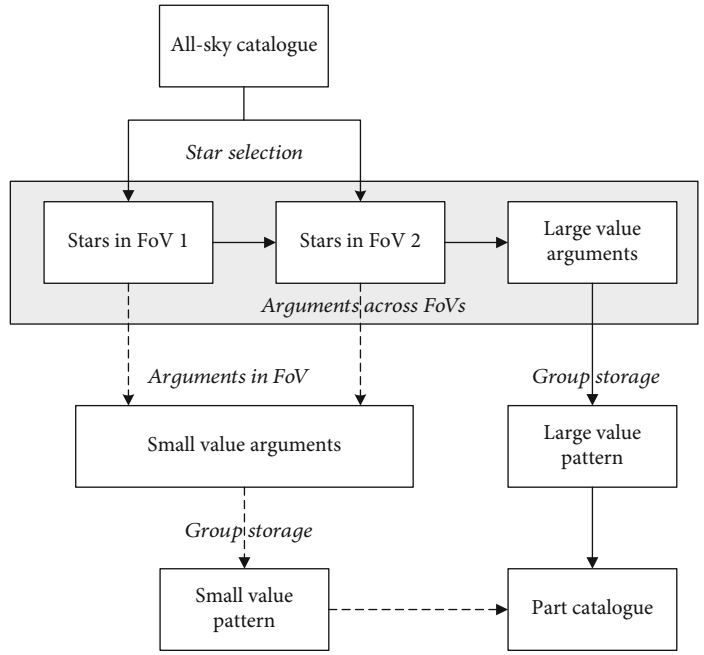

Figure 7: Dynamic establishment of the local star catalog.

aided star pattern matching process for distributed multiple FoVs is as follows:

Step 1. use the inertial information to estimate the LoS vector $\tilde{r}_n^i$ of each FoV

Step 2. calculate the error radius ΔR_n from the inertial errors and further obtain the catalog radius $\tilde{R}_n$ of each FoV

Step 3. utilize the LoS vector $\tilde{r}_n^i$ from Step 1 and two radii (ΔR_n and $\tilde{R}_n$) from Step 2 to select stars for each FoV from the all-sky catalog (external data) and then generate the part catalog in real time

Step 4. use the fused image (external data) and the part catalog from Step 3 to match the star pattern

4. Simulation Results and Analysis

4.1. Analysis of Star Observability Performance. In this section, we choose the double-FoV star sensor for a simulation experiment. The main parameters are shown in Table 1.

The installation angle is 60°. The all-sky catalog is based on the Smithsonian Astrophysical Observatory (SAO) with a 6.0 limited magnitude and double and variable star disposing. The simulation experiment is designed with ten thousand Monte Carlo star observations, and the numbers of visible stars in the main, auxiliary, and fused FoVs are recorded. The mean value results are shown in Figure 8.

Table 1: Parameters of the star sensor.

Parameter	Value
Focal length (mm)	54.95
Limited magnitude (M)	6
FoV size (°)	$4^\circ \times 4^\circ$

When the number of visible stars is below 3, star pattern matching does not work due to the triangle matching algorithm chosen in this paper. Thus, the number of instances that the number of visible stars is below 3 is counted for the different limited magnitudes. In particular, this number is also recorded when the number of visible stars is below 3 in both single FoVs but above 3 in the fused FoV (called remedy times). The results are all shown in Figure 9.

According to Figures 8 and 9, the stars in the fused FoV contain the stars in the main and auxiliary FoVs from the corresponding relationship. When the limited magnitude is

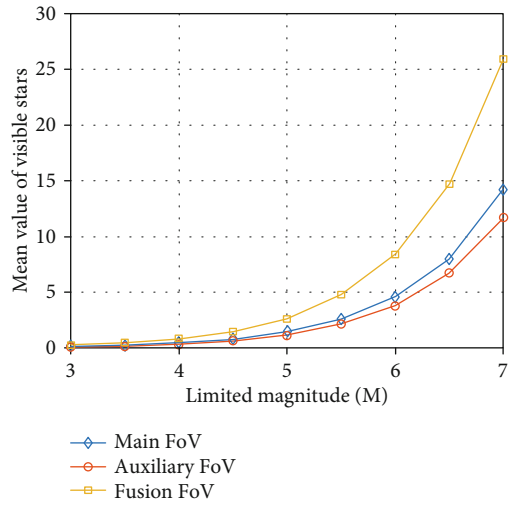

Figure 8: Mean value of visible stars for different FoVs.

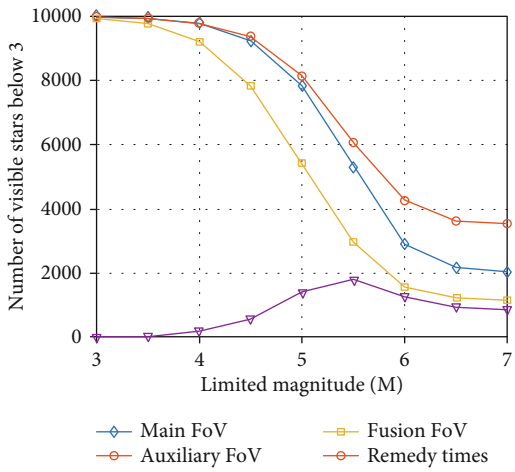

Figure 9: Numbers of instances of a number of visible stars below 3.

small (<5), there are a large number of results with a number of stars below 3 because the all-sky catalog has few stars for a small limited magnitude. At the same time, the remedy times are also small. As the magnitude increases, the number of visible stars in each FoV obviously increases. When the magnitude is 5, the remedy times reach a maximum, which corresponds to the number of stars above 3 in the fused FoV. When the magnitude is 6, each FoV basically satisfies the requirement for triangle matching. When the magnitude increases above 6, each FoV shows an obvious increase in the number of visible stars. However, on the contrary, the number of instances of a number of visible stars below 3 is reduced.

4.2. Analysis of the Observed Scope Prediction Performance. According to the inertial-aided star identification principle in Section 4, assistance information helps to estimate the LoS vector, but the errors affect the estimation accuracy and the number of stars that are the same in both the star image and catalog. Obviously, the more identical stars there are, the more successful the matching results will be. In addition, the influence of inertial errors on the LoS vector estimation is independent of the multi-FoV star sensor when there are no errors in the installation. Therefore, only a single FoV is analyzed in this section.

Table 2: Three gyroscope bias conditions.

Gyroscope bias condition	Gyroscope bias value
Cond. 1	0.004°/h
Cond. 2	1°/h
Cond. 3	5°/h

An error model of the inertial sensor is established. For a gyroscope, the errors are mainly due to the gyro drift error ε, which consists of a random constant ε_b, random errors of a first-order Markov process ε_r, and white noise w_g. For an accelerometer, its drift ∇_a is only due to a first-order Markov process. In addition, the error model is the same for the three axes in both the gyroscope and the accelerometer.

The value of the gyroscope bias is based on the value of SIGI in [1]. To compare the different influences on accuracy, three conditions (denoted by cond. hereafter) from high to low accuracy are given for the gyro in this section and shown in Table 2.

At the same time, the accelerometer bias is fixed at 100μg. The correlation times of the Markov process for the gyroscope and accelerometer are 3600 s and 1800 s, respectively.

The following variables are defined in this section to describe the degree of influence. The LoS vector bias angle is η_0. If a star image has N_O visible stars, having the same stars means that the stars exist in both the star image and the part catalog, whose number is N_{RP}. Thus, the rate of identical stars $_{\mathrm{COR}}$ is given by equation (16):

$$\mathrm{COR} = \frac{N_{\mathrm{RP}}}{N_O} \times 100\%. \tag{16}$$

However, the COR will be affected by the stars in the image. The COR concerns stars that do not have a strict uniform distribution in the all-sky catalog. Therefore, the number of stars affecting matching N_{ai} is given by equation (17):

$$N_{\mathrm{ai}} = N_O - N_{\mathrm{RP}}. \tag{17}$$

According to the simulation conditions, the experiment simulates an aerospace vehicle cruise. The influences of different gyroscope biases on the LoS bias angle, the COR and the number of stars affecting matching are shown in Figures 10–12, respectively.

From Figure 10, the LoS vector bias angle is minimum in cond. 1 (0.004°/h), and all the values are below 0.15° because the maximum gyroscope accuracy means that the assistance information does not diverge and hardly affects the accuracy of the estimated LoS. The results of cond. 2 (1°/h) are in the middle, and the maximum result of cond. 4 is below 3. The results of cond. 3 (5°/h) are the worst because the inertial positions and attitudes experience larger error accumulations, which is not small for this condition. The maximum

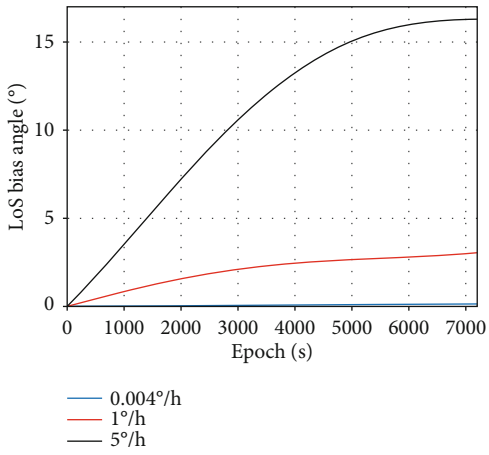

Figure 10: LoS vector bias angle for different gyroscope biases.

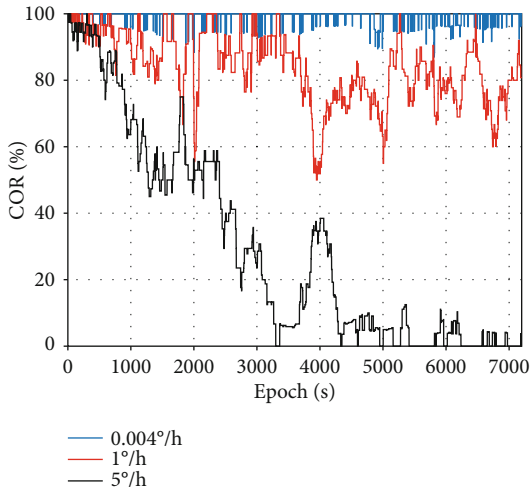

Figure 11: COR for different gyroscope biases.

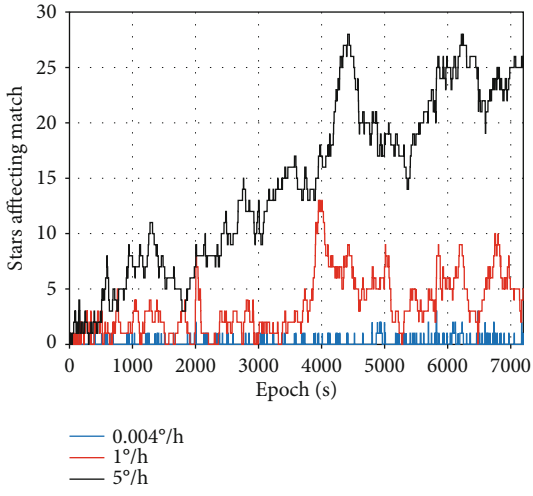

Figure 12: Number of stars affecting matching for different gyroscope biases.

is 16.30°, which is close to the FoV diameter ($12\sqrt{2}^{\circ} \approx 16.97^{\circ}$) and theoretically has a serious influence on the COR.

The situation of identical stars is shown in Figures 11 and 12. The results of cond. 3 (5°/h) are affected more strongly than the result of the other two conditions. The COR of cond. 3 exhibits a larger decrease in the fluctuation and is below 10% after 4300 s, which corresponds to the obvious increase in the number of stars affecting matching. The LoS bias angle has a limited influence on the COR of cond. 2, which is stable at approximately 80% at approximately 4000 s, corresponding to 5 stars affecting matching. The COR of cond. 1 (0.004°/h) is always above 80%, and the number of stars affecting matching is below 5.

Consider the 4060 s epoch as an example. The LoS vector is RA of 182.909° and Dec of 20.000°. The number of visible stars is 26. At this time, the results of the 5 conditions are shown in Table 3. The identical stars are shown in Figure 13.

From Table 3, in this epoch, the CORs of cond. 3 (5°/h) and cond. 2 (1°/h) are poor. The number of identical stars of cond.3 (5°/h) is very limited. Compared with the other 2 conditions, the number of identical stars is obviously reduced.

In addition, defining the matching success rate is the percent rate of the epochs with a correct identification in all the epochs. The success rates of the above three conditions are 98.80%, 88.58%, and 41.67%, respectively. The distribution of these success rates is similar to that of the LoS vector, bias angle, and the COR: the first condition gives the beset result, the second condition is in the middle, and the third condition gives the worst result.

4.3. Analysis of the Star Pattern Matching Performance. In this section, a simulation experiment is designed for the dynamic flight of an aerospace vehicle.

The main parameters of the double-FoV star sensor are shown in Table 1. The installation angle is 30°. A trace of the aerospace vehicle in cruise is simulated in Figure 14.

The number of visible stars and the main and auxiliary LoS vectors per second around the 3000 s trace are recorded, and the results are shown in Figures 15–17.

From Figure 15, the number of visible stars in the fused FoV exhibits a fluctuation. The mean number of stars is 5.4 (3.0 in the main FoV and 2.4 in the auxiliary FoV). During the whole simulation, there are 757 epochs with a number of visible stars below 3 in the fused FoV (1433 epochs in the main FoV and 1639 epochs in the auxiliary FoV), which shows that the fused FoV can efficiently extend the number of visible stars.

The matching success rate is 80.36% in the fused FoV. After calculating the statistics, the epochs with a number of visible stars below 5 mainly affect the success rate. The results of four epochs that can match are shown in in Figure 18.

From Figure 18, the star pattern matching algorithm for distributed FoVs can not only identify the stars only in a single FoV (in subgraphs (a) and (b)) but also provide opportunities to identify stars across FoVs (in subgraphs (c) and (d)). The algorithm takes full advantage of stars across multiple FoVs.

Table 3: Statistics in the 4060 s epoch for 5 conditions.

Accuracy condition	Estimated LoS		LoS bias angle (°)	COR	Part catalog stars	Identical stars
	RA (°)	Dec (°)				
0.004°/h	182.887	20.070	0.0739	100%	26	26
0.05°/h	182.887	19.749	0.2516	100%	26	26
0.1°/h	182.980	20.755	0.7577	96.15%	26	25
1°/h	181.397	17.988	2.4672	69.23%	27	18
5°/h	189.835	31.857	13.3845	38.46%	27	12

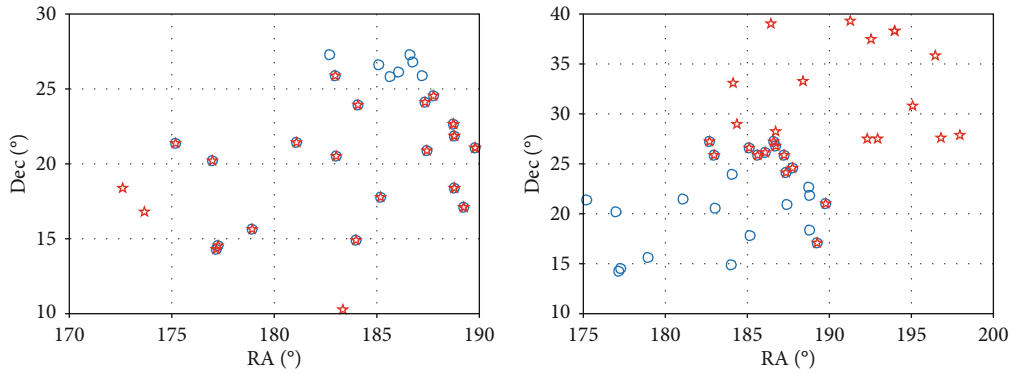

(a) Identical stars in cond. 4 (1°/h) (b) Identical stars in cond. 5 (5°/h)

Figure 13: The identical stars in the 4060 s epoch.

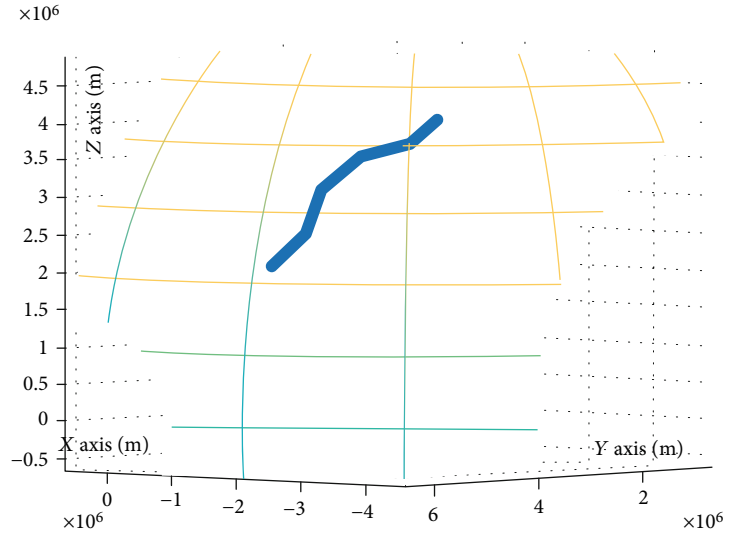

Figure 14: Cruise trace of an aerospace vehicle.

However, there is not a star image with stars existing in both the main and auxiliary FoVs for the single-FoV star sensor. Thus, a dynamic simulation is designed that chooses an installation angle of 45° and simulates the possible 100 attitudes in one position of an aerospace vehicle. The results of successful matching are shown in Figure 19.

From Figure 19, due to the small FoV (4° × 4°) and limited number of visible stars, approximately 50% of the matches fail (50 successful matches of 100 in the main FoV and 52 successful matches in the auxiliary FoV), for the whole trace. This means that star identification only in the single small FoV cannot provide robust output. In contrast, the fused FoV has a failure rate of approximately 10% (90

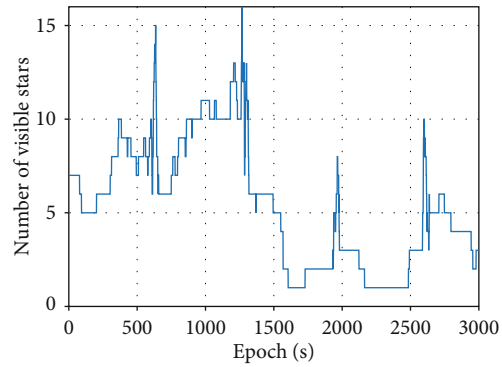

Figure 15: Number of visible stars in the fused FoV.

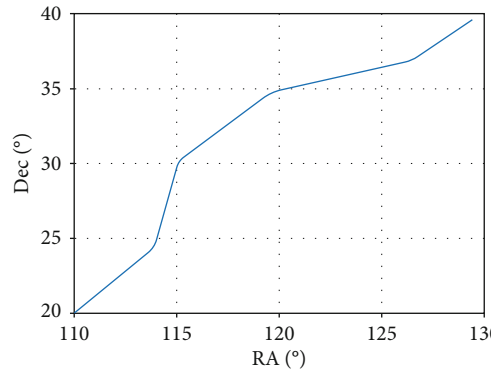

Figure 16: Main LoS vector.

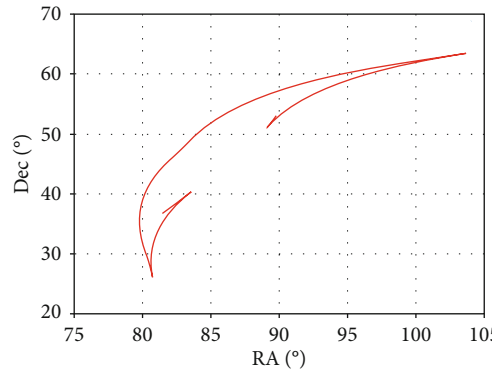

Figure 17: Auxiliary LoS vector.

successful matches in the fused FoV). This result proves the efficiency of the method.

As an evaluation of real-time performance, compared to conventional approaches, the dynamic local star catalog established by the proposed method and the conventional all-sky star catalog are compared in Figure 20.

In the proposed method, the optical axis direction is estimated based on inertial measurements, and then the multiple FoVs' observed scopes are estimated. Beneficial from the estimation of the observed scopes, the local star catalog for star pattern matching could be established dynamically, whose magnitude is significantly reduced, as shown in Figure 20. Thus, the real-time performance is improved than the conventional star pattern matching method based on all-sky star catalog.

In summary, the simulation above proves that the star identification method for distributed multiple FoVs can best utilize the visible stars in each FoV to increase the match success rate not only in a Monte Carlo simulation but also in a dynamic flight experiment.

5. Conclusions

An inertial-aided star pattern matching method for distributed multiple FoVs is proposed, because the existing method

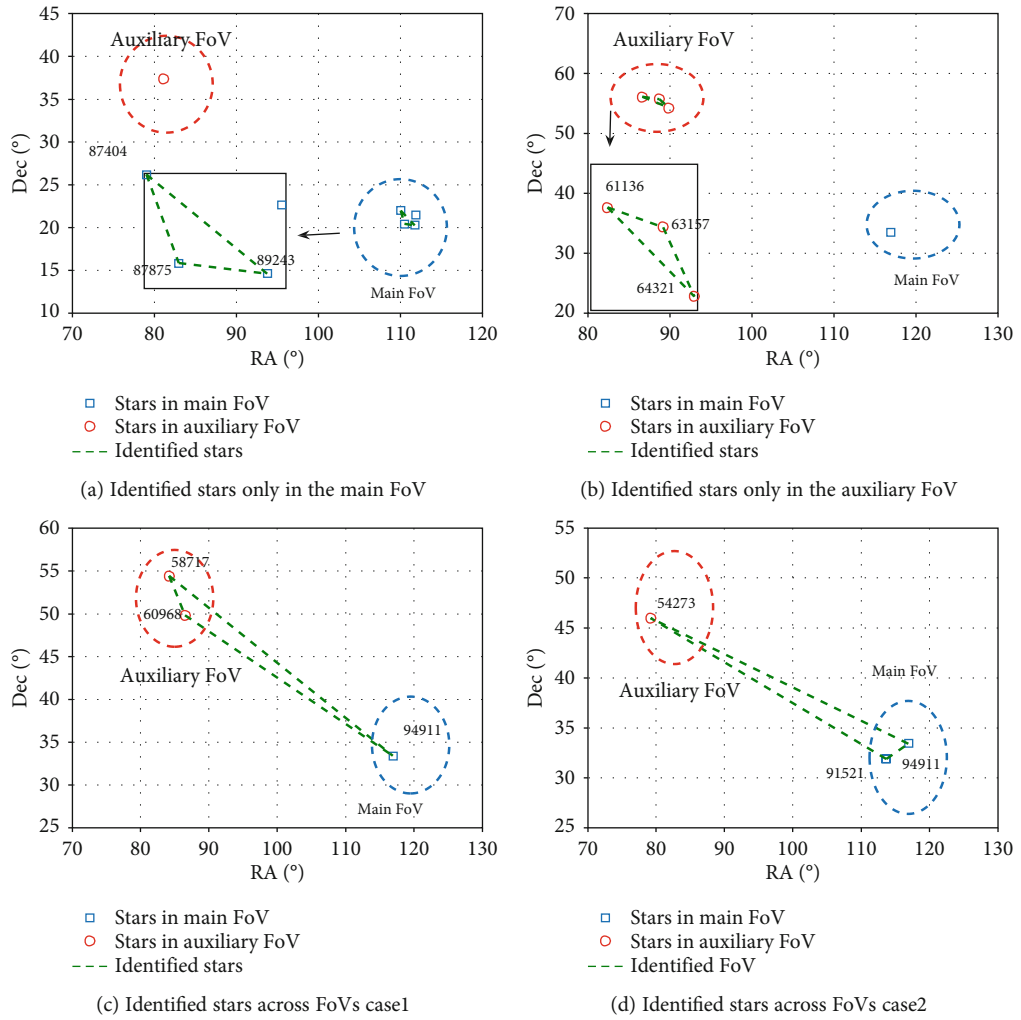

Figure 18: Four kinds of epoch for matching.

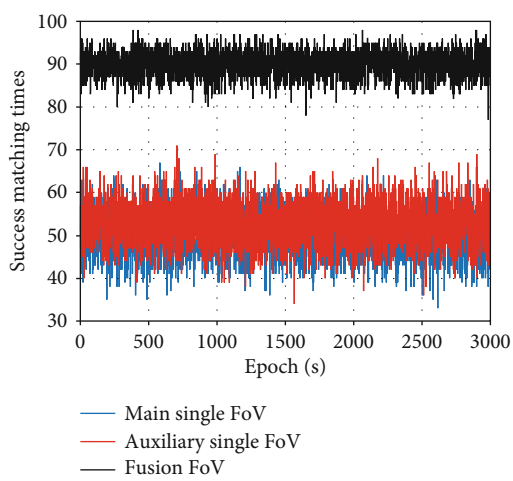

Figure 19: Number of successful matching for the whole trace.

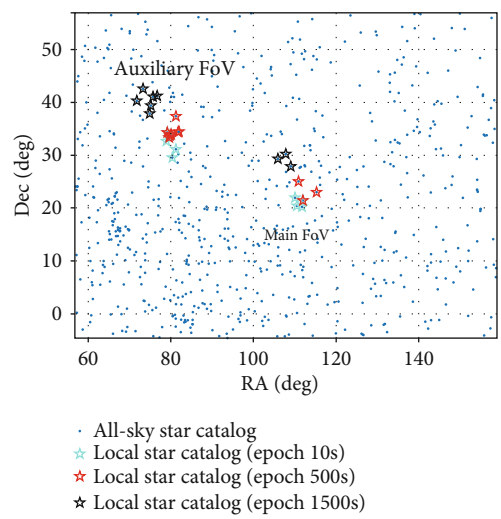

Figure 20: Comparison of dynamic local star catalog and all-sky star catalog.

for multiple FoVs cannot provide a continuous and robust star vector for an aerospace vehicle in cruise. First, the matching scheme is researched in the analysis of a distributed multi-FoV CNS. Then, the observation model for a multi-FoV star sensor is presented. Next, a specific matching method is proposed on the basis of LoS vector estimation and the dynamic establishment of a part catalog. Finally,

simulation experiments are designed to prove the efficiency of the matching method and robustness for an aerospace vehicle. The results from the simulation will help realize autonomous star identification for aerospace vehicles.

Data Availability

The authors declare that simulation data used to support the findings of this study in manuscript 2676210 titled \"A Novel Inertial-aided Star Pattern Matching Method for Distributed Multiple FoVs\" are included within the article.

Conflicts of Interest

The authors declared no potential conflicts of interest with respect to the research, authorship, and/or publication of this article.

Acknowledgments

This work was partially supported by the National Natural Science Foundation of China (Grant Nos. 61703208, 61533009, 61673208, 61873125, and 61533008), the Foundation Research Project of Jiangsu Province (the Natural Science Foundation of Jiangsu Province, Grant Nos. BK20170815, BK20170767, and BK20181291), the Aeronautic Science Foundation of China (Grant No. 20165552043), the Science and Technology Innovation Project for the Selected Returned Overseas Chinese Scholars in Nanjing, the Fundamental Research Funds for the Central Universities (Grant Nos. NZ2019007, NP2018108, NJ20170005, and NP2017209), the Advanced Research Project of the Equipment Development (30102080101), the "333 project" in Jiangsu Province (Grant No. BRA2016405), the Scientific Research Foundation for the Selected Returned Overseas Chinese Scholars (Grant No. 2016), the peak of six personnel in Jiangsu Province (Grant No. 2013-JY-013), the Foundation of Key Laboratory of Navigation, Guidance and Health-Management Technologies of Advanced Aerocraft (Nanjing Univ. of Aeronautics and Astronautics), Ministry of Industry and Information Technology, Jiangsu Key Laboratory "Internet of Things and Control Technologies,"and the Priority Academic Program Development of Jiangsu Higher Education Institutions, Science and Technology on Avionics Integration Laboratory.

References

[1] A. Grantza, "X-37B orbital test vehicle and derivatives," in *AIAA SPACE 2011 Conference & Exposition*, pp. 1–14, Long Beach, California, 2011.

[2] X. Zhi, L. Jian-ye, Y. Feng, and C. Hai-ming, "Research of airborne INS/CNS integrated filtering algorithm based on celestial angle observation," *Journal of Astronautics*, vol. 2, no. 31, pp. 397–403, 2010.

[3] V. A. Muruganandan, J. H. Park, S. Lee, I.-S. Jeung, S. Kim, and G. Ju, "Development of the arcsecond pico star tracker (APST)," *Transactions of the Japan Society for Aeronautical and Space Sciences*, vol. 60, no. 6, pp. 355–365, 2017.

[4] T. Bank, "Analysis of the CT-633 star tracker's attitude estimation capability," *Guidance & Control*, vol. 5, no. 2, pp. 179–198, 1997.

[5] R. W. H. van Bezooijen, "SIRTF autonomous star tracker," *International Society for Optical Engineering*, vol. 4850, pp. 108–121, 2003.

[6] C. C. Liebe, "Pattern recognition of star constellations for spacecraft applications," *IEEE Aerospace and Electronic Systems Magazine*, vol. 8, no. 1, pp. 31–39, 1993.

[7] D. S. Mehta, S. Chen, and K. S. Low, "A robust star identification algorithm with star shortlisting," *Advances in Space Research*, vol. 61, no. 10, pp. 2647–2660, 2018.

[8] H. Yoon, S. W. Paek, Y. Lim, B. H. Lee, and H. Lee, "New star pattern identification with vector pattern matching for attitude determination," *IEEE Transactions on Aerospace and Electronic Systems*, vol. 49, no. 2, pp. 1108–1118, 2013.

[9] B. V. Sheela, C. Shekhar, P. Padmanabhan, and M. G. Chandrasekhar, "New star identification technique for attitude control," *Journal of Guidance, Control, and Dynamics*, vol. 14, no. 2, pp. 477–480, 1991.

[10] K. Ho, "A survey of algorithms for star identification with low-cost star trackers," *Acta Astronautica*, vol. 73, pp. 156–163, 2012.

[11] J. D. Trolinger and W. C. Rose, "Technique for simulating and evaluating aero-optical effects in optical systems," in *42nd AIAA Aerospace Sciences Meeting and Exhibit*, pp. 1–11, Reno, USA, 2004.

[12] Z. Wang, W. Xinguo, and Z. Guangjun, "Structure optimization for multi-FOV star sensors," *Infrared and Laser Engineering*, vol. 40, no. 12, pp. 2469–2473, 2011.

[13] D. Mortari, M. A. Samaan, C. Bruccoleri, and J. L. Junkins, "The pyramid star identification technique," *Navigation*, vol. 51, no. 3, pp. 171–183, 2004.

[14] D. Mortari and J. L. Junkins, "SP-search star pattern recognition for multiple fields of view star trackers," in *The 9th AAS/AIAA Space Flight Mechanics Meeting*, pp. 1–10, Breckenridge, USA, 1999.

[15] D. Mortari and A. Romoli, "StarNav III: a three fields of views star tracker," in *Proceedings, IEEE Aerospace Conference*, pp. 1–11, Big sky, USA, 2002.

[16] L. Blarre, N. Perrimon, and S. Airey, "New multiple head star sensor (HYDRA) description and status," in *AIAA Guidance, Navigation, and Control Conference and Exhibit*, pp. 1–9, San Francisco, California, USA, 2005.

[17] V. Ethier, P. Andrist, A. Babbitt, M. Pfaff, G. Rios-Georgio, and T. Welter, "DEbris capture and orbital manipulation – DECOM," in *AIAA SPACE 2011 Conference & Exposition*, Long Beach, California, USA, 2011.

[18] W. Zhang, W. Quan, and L. Guo, "Blurred star image processing for star sensors under dynamic conditions," *Sensors*, vol. 12, no. 5, pp. 6712–6726, 2012.

[19] M. A. Samann, D. Mortari, and J. L. Junkins, "Recursive mode star identification algorithms," *IEEE Transactions on Aerospace and Electronic Systems*, vol. 41, no. 4, pp. 1246–1254, 2005.

[20] Y. Cheng, J. L. Crassidis, and F. L. Markley, "Attitude estimation for large field-of-view sensors," *The Journal of the Astronautical Sciences*, vol. 54, no. 3-4, pp. 433–448, 2006.

[21] Y. Cao, R. Wang, J. Liu, and Z. Xiong, "A fast star identification method assisted by INS with stars geometric configuration for aerospace vehicle navigation," in *2018 IEEE/CSAA Guidance, Navigation and Control Conference (IEEE/CSAA GNCC)*, Xiamen, China, 2018.

[22] C. Jekeli, *Inertial navigation systems with geodetic applications*, Walter de Gruyter, 2012.